remote sensing

MDPI

Article

Estimating the Applicability of NDVI and SIF to Gross Primary Productivity and Grain-Yield Monitoring in China

Zhaoqiang Zhou [1,2], Yibo Ding [3], Suning Liu [4], Yao Wang [1,2], Qiang Fu [5] and Haiyun Shi [1,2,*]

[1] State Environmental Protection Key Laboratory of Integrated Surface Water-Groundwater Pollution Control, School of Environmental Science and Engineering, Southern University of Science and Technology, Shenzhen 518055, China; 11930942@mail.sustech.edu.cn (Z.Z.); 12131078@mail.sustech.edu.cn (Y.W.)
[2] Guangdong Provincial Key Laboratory of Soil and Groundwater Pollution Control, School of Environmental Science and Engineering, Southern University of Science and Technology, Shenzhen 518055, China
[3] Yellow River Engineering Consulting Co. Ltd., Zhengzhou 450003, China; dingyiboxbnl@nwafu.edu.cn
[4] Center for Climate Physics, Institute for Basic Science, Busan 46241, Korea; u3002906@connect.hku.hk
[5] School of Water Conservancy and Civil Engineering, Northeast Agricultural University, Harbin 150006, China; fuqiang@neau.edu.cn
* Correspondence: shihy@sustech.edu.cn; Tel.: +86-755-88018870

Abstract: Vegetation, a key intermediary linking water, the atmosphere, and the ground, performs extremely important functions in nature and for our existence. Although satellite-based remote-sensing technologies have become important for monitoring vegetation dynamics, selecting the correct remote-sensing vegetation indicator has become paramount for such investigations. This study investigated the consistencies between a photosynthetic activity index (the solar-induced chlorophyll fluorescence (SIF) indicator) and the traditional vegetation index (the Normalized Difference Vegetation Index (NDVI)) among different land-cover types and in different seasons and explored the applicability of NDVI and SIF in different cases by comparing their performances in gross primary production (GPP) and grain-yield-monitoring applications. The vegetation cover and photosynthesis showed decreasing trends, which were mainly concentrated in northern Xinjiang and part of the Qinghai–Tibet Plateau; a decreasing trend was also identified in a small part of Northeast China. The correlations between NDVI and SIF were strong for all land-cover types except evergreen needleleaf forests and evergreen broadleaf forests. Compared with NDVI, SIF had some advantages when monitoring the GPP and grain yields among different land-cover types. For example, SIF could capture the effects of drought on GPP and grain yields better than NDVI. To summarize, as the temporal extent of the available SIF data is extended, SIF will certainly perform increasingly wide applications in agricultural-management research that is closely related to GPP and grain-yield monitoring.

Keywords: Normalized Difference Vegetation Index; solar-induced chlorophyll fluorescence; gross primary production; grain yield; China

Citation: Zhou, Z.; Ding, Y.; Liu, S.; Wang, Y.; Fu, Q.; Shi, H. Estimating the Applicability of NDVI and SIF to Gross Primary Productivity and Grain-Yield Monitoring in China. *Remote Sens.* **2022**, *14*, 3237. https://doi.org/10.3390/rs14133237

Academic Editor: Ranjeet John

Received: 1 June 2022
Accepted: 4 July 2022
Published: 5 July 2022

1. Introduction

The varieties and sizes of natural ecosystems are largely influenced by natural vegetation [1–5]. Vegetation also plays an important role in influencing human survival; for example, vegetation produces oxygen via photosynthesis [6], provides resources (e.g., food and timber) [7–9], regulates atmospheric circulation [3], affects climate change [10], and reduces soil erosion [11,12]. Therefore, monitoring vegetation conditions, especially vegetation changes, is of great significance, as this information is important for protecting the natural environment [2,13].

Several methods have been developed to monitor field vegetation [14,15]. Spot sampling is typically used in the early stages of vegetation monitoring [16,17] and has a high

level of accuracy and reliability [17]. This method can even be used to evaluate the accuracies of other methods [18]. For example, Liu et al. [18] provided sampling protocols to effectively improve the estimation accuracy of the forest leaf area index. However, spot sampling has some disadvantages; it is not a continuous vegetation monitor [17], it is unsuitable for monitoring vegetation over a large area [19], and it requires substantial resources (time and materials) [17]. With the development of remote-sensing technologies, vegetation changes can be effectively monitored by using equipment carried on various platforms, such as unmanned aerial vehicles, aircrafts, and satellites [15,20,21]. For example, Wei et al. [15] used an unmanned aerial vehicle to monitor the vegetation dynamics in the foreland of the Urumqi Glacier, and Chang et al. [21] used an unmanned aerial system to monitor corn and soybean crops on the Cornell Musgrave Research Farm in New York, USA. Different global-scale, satellite-derived datasets were used by Ye et al. [13] to compare trends in vegetation seasonality. The rapid development of satellite technologies has resulted in the availability of time-series products with higher precision and longer temporal domains [14,22,23]. Many vegetation indicators have been used to describe vegetation characteristics, such as Normalized Difference Vegetation Index (NDVI) [24], Vegetation Condition Index [25], Vegetation Health Index [26], Enhanced Vegetation Index [27] and solar-induced chlorophyll fluorescence (SIF) [14].

Among the above vegetation indicators, NDVI and SIF have been widely used to describe vegetation dynamics in drought and crop-yield studies [4,13,14,28,29]. Regarding drought research, Ding et al. [29] employed NDVI to reveal the effects of agricultural drought on forest, grassland, and cropland ecosystems over China, and Xu et al. [30] used NDVI to obtain the response time and degree of vegetation to meteorological drought conditions in North China. Liu et al. [31] applied SIF to analyze the sensitivity of vegetation in the Hulun Buir Grassland, China, and indicated that SIF was more sensitive than NDVI when monitoring the responses of vegetation to drought. Chen et al. [28] recorded the changing biomass features of vegetation during the 2009/2010 droughts over the North China Plain, based on SIF. Among existing studies on crop yields, Kern et al. [7] employed NDVI to forecast early crop yields in Central Europe, and Peña-Gallardo et al. [8] used NDVI to analyze the response times of the yields of different crops (barley, winter wheat, soybean, corn, and cotton) to drought in the USA. Chen et al. [28] analyzed the relations between SIF, crop yield, and the gross primary productivity (GPP) of vegetation during the growth periods of summer maize over the North China Plain. Chang et al. [21] used both NDVI and SIF to identify seasonal changes in corn and soybean croplands in New York, USA. Although NDVI and SIF have already been applied in vegetation research, estimating GPP and crop yield by using SIF data combined with statistical methods is still not a common practice, mainly due to the low spatial resolution of the available SIF data. Li and Xiao [14] developed a global SIF dataset (GOSIF) with high spatial and temporal resolutions (0.05° and 8 days, respectively) representing the 2000–2020 period; this dataset could broaden the use of SIF studies over longer time periods and at higher resolutions. Although previous studies on NDVI and SIF have been conducted in research fields such as the response of vegetation to drought [32], the phenology of vegetation in high-latitude forests [33], and the relationship between GPP and SIF [4], NDVI and SIF have not been thoroughly compared due to limitations in existing research, such as a small study area [34], the analysis of only a single vegetation type [33], or the lack of measured crop-yield data [32].

Therefore, this study aims to examine the performances of NDVI and SIF from 2001–2019 in a large study area (China) for various land-cover types based on measured grain-yield data. The primary objectives of this study are (1) to explore the response relationship between NDVI and SIF; (2) to check whether SIF has an advantage over NDVI in GPP monitoring applications; and (3) to compare the application of SIF and NDVI in grain-yield monitoring. The obtained results represent systematic performance differences between NDVI and SIF and provide a reference for selecting suitable vegetation-monitoring indicators in future vegetation studies.

2. Data and Methods

2.1. Study Area

China is located in East Asia (3°51′N−53°33′N and 73°29′E−135°04′E) and has an approximate land area of 9.63 × 10^6 km^2 and a sea area of 3.00 × 10^6 km^2 [35]. The main plain regions in China include the Northeast Plain (NEP), the North China Plain (NCP), and the middle-lower reaches of the Yangtze River Plain (MLRYR); the main plateau regions include the Inner Mongolia Plateau, the Loess Plateau (LP), the Qinghai–Tibet Plateau (QTP), and the Yun-Gui Plateau (YGP). The main basins in China include the Sichuan Basin (SCB), the Dzungarian Basin, and the Tarim Basin (Figure 1a). Based on the regional characteristics of China, the major crop production areas (croplands) can be divided into nine subregions (http://www.resdc.cn/data.aspx?DATAID=275, accessed on 21 October 2021): the NEP, NCP, MLRYR, YGP, SCB, LP, QTP, southern China (SC), and arid and semiarid northern China (ASANC) (Figure 1c).

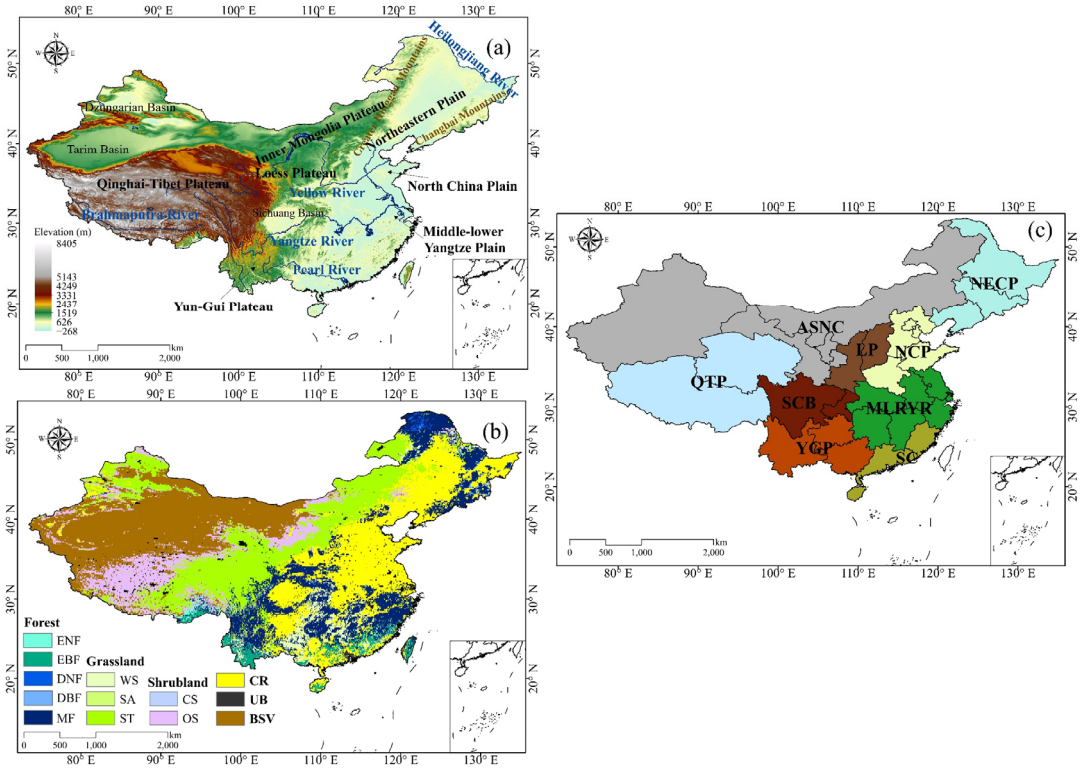

Figure 1. (**a**) Topographic and geographic zones of China; (**b**) land-cover types of China; and (**c**) the nine major crop production areas of China.

The land-cover map used herein was derived from the Moderate-Resolution Imaging Spectroradiometer (MODIS) land-cover-type product (MCD12C1) and was based on the International Geosphere-Biosphere Programme (IGBP) classification scheme. The MCD12C1 product released in 2019 was used to classify different land-cover types without considering the land-cover-type changes that occurred during the 2001–2019 study period, and the proportions of different land-cover types were calculated (Table 1). The evergreen needleleaf forest (ENF) and evergreen broadleaf forest (EBF) land-cover types were mainly located in southwestern China; the deciduous needleleaf forest (DNF) and deciduous broadleaf forest (DBF) land-cover types were mainly located in northeastern China; mixed forests (MF) were mainly located in northeastern, southwestern (YGP), and southeastern China; closed shrublands (CS) were mainly located in southwestern (YGP) China; open shrublands (OS) were mainly located in western (QTP and Tarim Basin) and northern (Inner Mongolia Plateau) China; woody savannas (WS) were mainly located in southwestern (YGP) and

southeastern China; savannas (SA) were mainly located in northeastern China; and steppes (ST) were mainly located in northeastern, northern (Inner Mongolia Plateau), northwestern (Tarim Basin), and southwestern (QTP) China. Croplands were mainly located in northeastern (NEP), northern (NCP), and southwestern (SCB) China. Urban and built-up (UB) areas were dispersed across China. Barren or sparsely vegetated (BSV) areas were mainly located in the northwestern part of China (Figure 1b). The percentage of the cultivated area in each crop production area is 58.47% (NEP), 82.26% (NCP), 44.01% (MLRYR), 31.53% (SC), 28.70% (YGP), 26.20% (SCB), 44.42% (LP), 7.752% (ASANC), and 0.70% (QTP).

Table 1. Proportions of different land-cover types.

Vegetation Type		Abbreviation
Class 1	**Class 2**	
Forest (17.85%)	Evergreen needleleaf forest (3.22%)	ENF
	Evergreen broadleaf forest (12.43%)	EBF
	Deciduous needleleaf forest (1.20%)	DNF
	Deciduous broadleaf forest (2.04%)	DBF
	Mixed forest (81.11%)	MF
Shrubland (10.21%)	Closed shrublands (0.69%)	CS
	Open shrublands (99.31%)	OS
Grassland (24.05%)	Woody savannas (14.51%)	WS
	Savannas (0.24%)	SA
	Steppes (85.25%)	ST
Croplands (23.28%)		CR
Urban and built-up areas (0.81%)		UB
Barren or sparsely vegetated areas (23.80%)		BSV

2.2. Datasets

In this study, monthly SIF data recorded from 2001–2019 were obtained from a high-resolution GOSIF product (https://globalecology.unh.edu//data/GOSIF.html, accessed on 21 October 2021). The GOSIF records were retrieved from the original Orbiting Carbon Observatory (OCO)-2 SIF retrievals using a machine-learning model and other finer-scale data as inputs. Compared with the original OCO-2 SIF data, the spatial distribution of and seasonal variation in the GOSIF dataset were consistent with the corresponding characteristics of the coarse SIF data directly collected by OCO-2 SIF. However, the GOSIF data had a higher temporal resolution (8 days) and a higher spatial resolution (0.05°), which was of great significance for using SIF data to study the global carbon cycle. Meanwhile, GOSIF data covering the world were of great significance for exploring the role of SIF in drought monitoring, vegetation phenology, and stress monitoring [36,37]. For a detailed description of the GOSIF dataset, please refer to Li and Xiao [14].

In East Asia, the eddy correlation flux-tower measurements are less readily available [38]. Since the flux-tower distribution is uneven and sparse, it is impossible to obtain high-precision GPP in global range. Many scholars have evaluated the MODIS GPP through ground observation sites [14,36]. Although the MODIS GPP may overestimate or underestimate the tower eddy-flux network measurements, the MODIS product can reproduce seasonal and spatial changes well [39]. Since the purpose of this study was to evaluate the spatial monitoring performance of GOSIF in fine resolutions, we chose MODIS GPP (MOD17A2H) in this study. GPP calculation was based on the LUE Model. The specific calculation process can be referred to Zhao et al. [40]. MODIS GPP (MOD17A2H) produces (2001–2019) were obtained from MODIS (https://modis.gsfc.nasa.gov/data/, accessed on 21 October 2021). GPP data had a spatial resolution of 500 m and a temporal resolution of 8 days.

In this study, we used the ability of NDVI to monitor vegetation dynamics, GPP and drought [5,41,42] to compare the application potential of GOSIF. NDVI captured the contrast in reflectance between the red and near-infrared radiance wavelengths. NDVI (MOD13C2) data (2001–2019) were obtained from MODIS (https://modis.gsfc.nasa.gov/data/, accessed on 21 October 2021). The NDVI data had a spatial resolution of 0.05° and a temporal resolution of 1 month.

Per-unit grain yields were obtained by dividing grain yield and cropland area. Grain yields and cropland area data recorded from 2001 to 2019 were acquired from China's agricultural statistical data and the 60 years' agricultural statistical data of the Ministry of Agriculture and Rural Affairs of China (http://zdscxx.moa.gov.cn:8080/nyb/pc/index.jsp, accessed on 21 October 2021) and the China Statistical Yearbook published by the National Bureau of statistics (http://www.stats.gov.cn/tjsj/ndsj/, accessed on 21 October 2021). To ensure consistency among the spatiotemporal resolutions of the SIF, NDVI, and GPP data, the GPP data were resampled to a spatial resolution of 0.05°, and the 8-day GOSIF and GPP data were resampled to the monthly scale [32].

2.3. Analysis

The Pearson correlation coefficient (PCC) was calculated between SIF and NDVI [43]. The relations between monthly SIF and NDVI were explored across different land cover types and in different seasons. We selected a correlation coefficient that passed the significance level of $p < 0.05$. For two time series, x and y, the PCC was calculated as follows:

$$\mathrm{PCC} = \frac{\sum_{i=1}^{n}(x_i - \overline{x})(y_i - \overline{y})}{\sqrt{\sum_{i=1}^{n}(x_i - \overline{x})^2}\sqrt{\sum_{i=1}^{n}(y_i - \overline{y})^2}} \quad (1)$$

where x_i and y_i denote the i-th value in the two corresponding time series (monthly NDVI and SIF across different land-cover types and in different seasons). The PCC values range from –1 to 1. A PCC value greater than 0 indicates a positive linear correlation, a PCC value less than 0 indicates a negative linear correlation, and a PCC value equal to 0 indicates no linear correlation.

Next, we calculated the PCC values between monthly SIF (NDVI) and GPP. The temporal and spatial differences between SIF or NDVI and GPP were analyzed across different land-cover types and in different seasons to reveal the applicability of SIF and NDVI for monitoring GPP.

Finally, polynomial fitting (univariate quadratic function) was used to reveal the relationship between SIF (NDVI) and the per-unit grain yield. The coefficient of determination (R^2) was used to represent the abilities of the analyzed vegetation indicators to explain the measured changes in grain yield. Next, considering that China experienced relatively large-scale drought events during the 2009–2010 period, we compared the percentage changes in the SIF, NDVI, and per-unit grain yield values from 2009–2010 with the mean annual values recorded from 2001–2019 to reveal the abilities of NDVI and SIF to monitor grain-yield changes induced by drought. In addition, based on previous studies [5,29,35], in this study, spring, summer, autumn, and the growing season were defined as the periods from March to May, from June to August, from September to November, and from March to October, respectively.

3. Results

3.1. Consistency between SIF and NDVI

The seasonal spatial distributions of the PCC values obtained between NDVI and SIF are shown in Figure 2. During the growing season, lower degrees of consistency (PCC values < 0.8) were found in the SC, YGP, part of the SCB, MLRYR, QTP, and ASANC, while higher degrees of consistency were found in the NEP, NCP, LP, part of the SCB, and QTP (Figure 2a). The spatial distributions of the PCC in spring and autumn were similar to that in the growing season (Figure 2b,d). In summer, higher degrees of consistency

were found in part of the NEP, NCP, LP, and QTP (Figure 3c). In general, the degrees of consistency in summer were smaller than in other seasons.

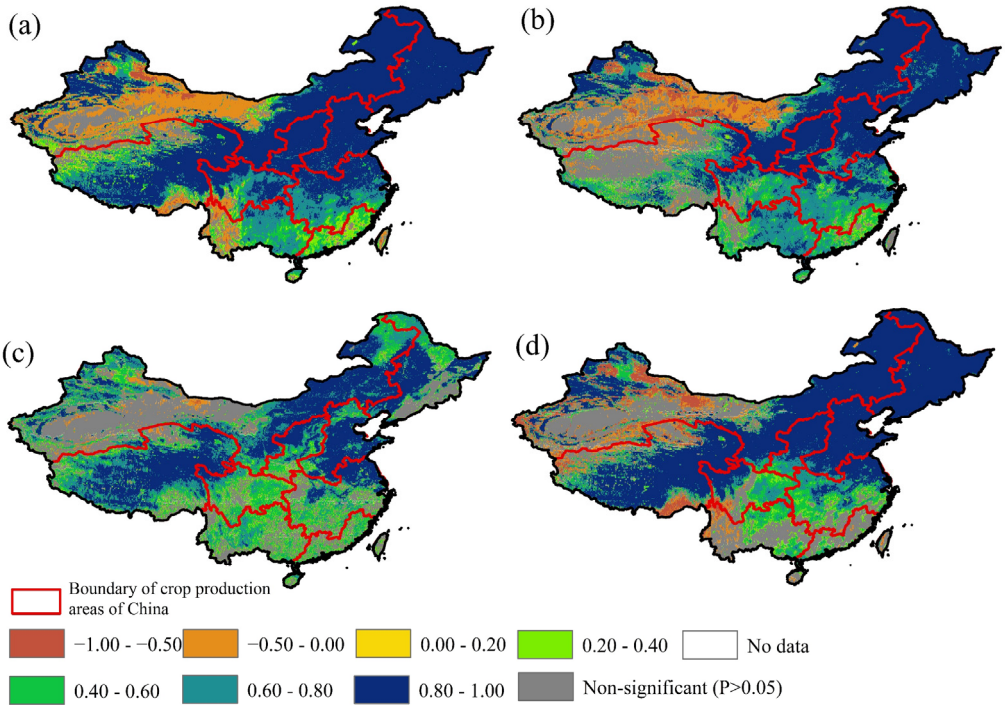

Figure 2. Seasonal spatial distributions of the PCC values obtained between NDVI and SIF: (**a**) growing season; (**b**) spring; (**c**) summer; and (**d**) autumn.

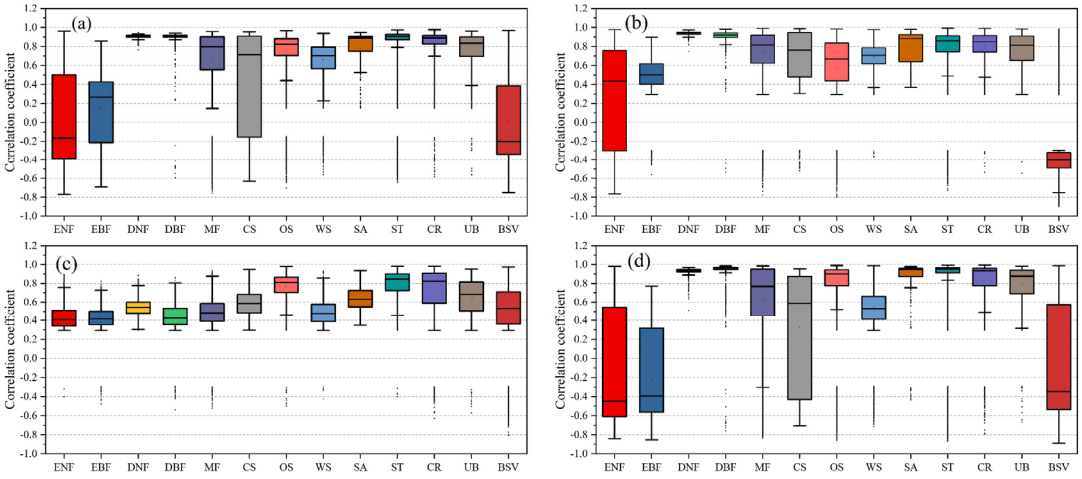

Figure 3. Seasonal PCC values obtained between NDVI and SIF for different land-cover types: (**a**) growing season; (**b**) spring; (**c**) summer; and (**d**) autumn.

To further analyze the relationship between the SIF and the NDVI, Figure 3 shows the correlations between the NDVI and the SIF obtained for different land-cover types during the growing season, spring, summer, and autumn. Overall, the correlations between the NDVI and the SIF differed significantly among different land-cover types. Figure 3a indicates that, except for the ENF, EBF, CS, and BSV land-cover types, during the growing season, the NDVI and the SIF showed relatively large positive correlations, and the PCC values were basically greater than 0.6. During spring, except for in the ENF, EBF, and BSV land-cover types, the NDVI and SIF showed relatively large positive correlations (Figure 3b). Compared to the springtime correlations, the summertime correlations between the NDVI

and the SIF were weak, with the PCC values mainly concentrated in the range of 0.4–0.6 (Figure 3c). In autumn, the relationships between the NDVI and the SIF for different land-cover types were similar to those obtained during spring; the correlations between NDVI and SIF in the ENF, EBF, CS, and BSV land-cover types were relatively weak during autumn. In the land-cover types other than the ENF and EBF, the correlations between the NDVI and the SIF revealed larger PCC values (Figure 3d). In general, the correlations between the NDVI and the SIF were stronger in regions comprising other land-cover types compared to the correlations obtained in the ENF, EBF, and BSV regions.

3.2. Relationships between SIF and GPP and between NDVI and GPP

Figure 4 shows the spatial distributions of the correlations between the SIF (NDVI) and the GPP obtained in different seasons. During the growing season, the PCC values (Figure 4a,e) mainly ranged from 0.80 to 1.00 (for SIF) and from 0.20 to 0.60 (for NDVI) in the SC. In the YGP, the PCC values ranged from 0.80 to 1.00 (for SIF) and from −0.50 to 0.80 (for the NDVI). The SIF had a higher degree of consistency with the GPP than the NDVI during the growing season. During spring, negative PCC values were found in the western YGP and QTP regions (Figure 4b,f), indicating that the SIF had a higher degree of consistency with the GPP than the NDVI did in southwestern China. There was a large amount of BSV coverage in the northwestern part of China, and GPP data were missing in these areas [4,28]. The missing data resulted in gaps in coverage for the northwestern part of China. The relations between the SIF (NDVI) and the GPP during the other two seasons were similar to those identified during the growing season.

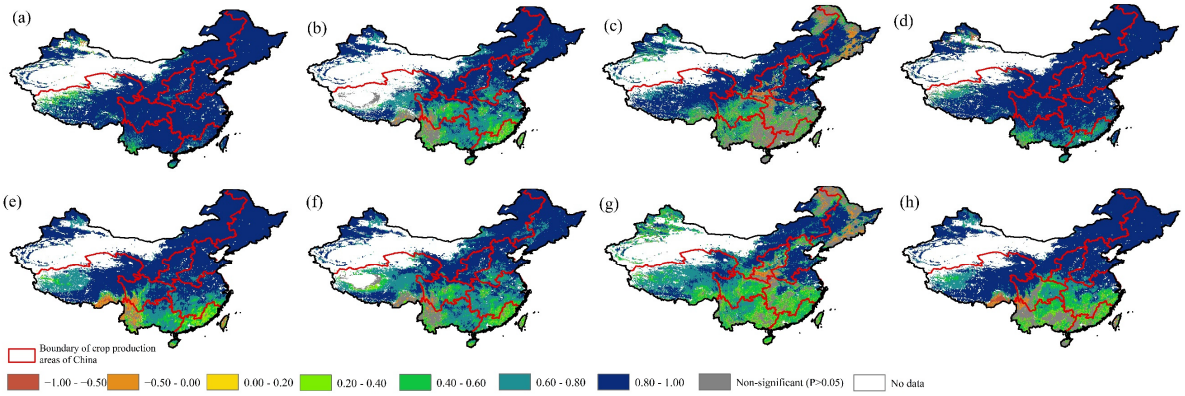

Figure 4. Spatial distributions of the correlations between GPP and SIF ((**a**) growing season; (**b**) spring; (**c**) summer; and (**d**) autumn) and between GPP and NDVI ((**e**) growing season; (**f**) spring; (**g**) summer; and (**h**) autumn).

To further analyze the relationships between the SIF (NDVI) and the GPP, the correlations between the SIF (NDVI) and the GPP were calculated for different land-cover types, as shown in Figure 5. As shown in Figure 5a, during the growing season, the SIF and the GPP showed relatively strong correlations for most of the land-cover types except for the EBF and the BSV; the NDVI and GPP also showed high correlations for most of the land-cover types except for the ENF, EBF, and CS. However, the PCC values derived between the SIF and the GPP were essentially greater and less variable than those obtained between the NDVI and the GPP. During spring (Figure 5b), a significant correlation was found between the SIF and the GPP, while the correlation between the NDVI and the GPP was relatively small, and the fluctuation ranges of the PCC values were relatively large in the regions characterized by the ENF, EBF, DNF, and DBF land-cover types. During summer (Figure 5c), the PCC values obtained between the SIF (NDVI) and the GPP fluctuated widely. In particular, the correlations were all relatively small in regions characterized by forest vegetation types, and the fluctuation ranges were relatively large. During autumn (Figure 5d), the PCC values derived between the SIF and the GPP were large, while those

obtained between the NDVI and the GPP were smaller, especially in the regions comprising ENF, EBF, and CS vegetation. Overall, the correlations between the SIF and the GPP were more significant than those between the NDVI and the GPP.

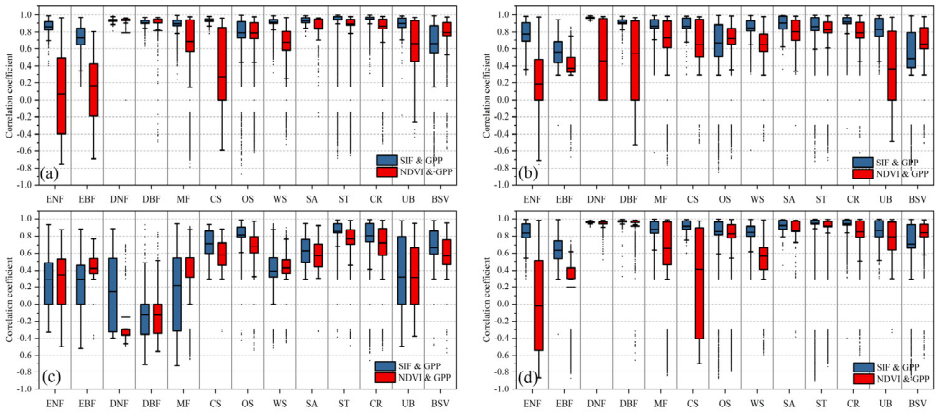

Figure 5. Correlations between SIF (NDVI) and GPP in regions with different land-cover types and in different seasons: (**a**) growing season; (**b**) spring; (**c**) summer; and (**d**) autumn.

3.3. Performances of SIF and NDVI in Grain-Yield Monitoring

To determine the applicability of the SIF and the NDVI for the grain-yield monitoring, we compared the relationships between the average SIF (NDVI) values and the per-unit grain yields during the growing season over different subregions (Figure 6). Figure 6a shows the correlations of the SIF and NDVI values with the per-unit grain yields over different subregions. The degrees of consistency between the two indicators and the per-unit grain yields indicated the existence of close relationships between the SIF and the per-unit grain yield and between the NDVI and the per-unit grain yield. The PCC values obtained between the SIF and the per-unit grain yield were generally higher than those obtained between the NDVI and the per-unit grain yield, especially over the NEP, NCP, MLRYR, YGP, and ASANC regions. Figure 6b shows the R^2 values obtained via polynomial fitting between the SIF (NDVI) and the per-unit grain yield. Except for in the QTP and MLRYR regions, the R^2 values obtained between the NDVI and the per-unit grain yield were greater than 0.8, while the R^2 values obtained between the SIF and the per-unit grain yield were greater than 0.8, except in the SC and QTP regions. Moreover, except in the SC, SCB, and QTP regions, the R^2 values derived between the NDVI and the per-unit grain yield were greater than those derived between the SIF and the per-unit grain yield. Although the SIF and the NDVI both showed good performances when monitoring the per-unit grain yield, and their performances were similar, the SIF had stronger correlations with the per-unit grain yield than the NDVI, indicating that the SIF could explain grain-yield changes better than the NDVI.

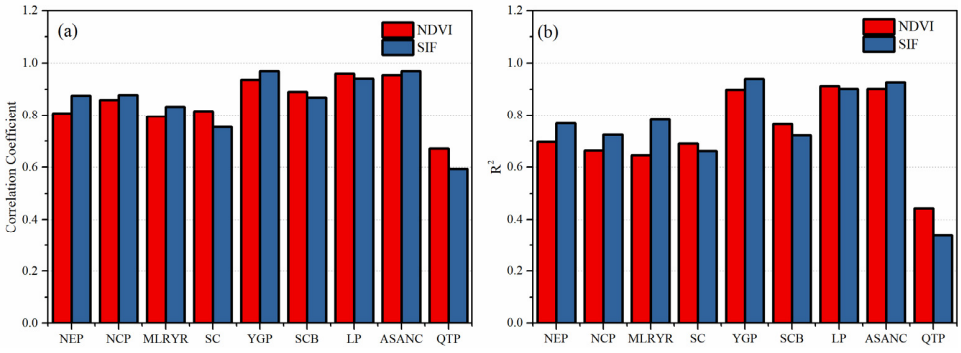

Figure 6. (**a**) PCC values and (**b**) R^2 values obtained between SIF (NDVI) and the per-unit grain yield during the growing season over different subregions.

Figure 7 shows the percentage changes in the SIF/NDVI/ per-unit grain yield during 2009–2010 compared with the corresponding mean annual values recorded from 2001–2019. In eight subregions, excluding the NEP, the percentage changes in the per-unit grain yield, SIF, and NDVI showed consistent increases or decreases from 2009–2010. In the NEP subregion, the percentage changes in the per-unit grain yield and the SIF increased from 2009–2010, but the NDVI percentage change decreased. Except in the NEP region, the SIF change rate was larger than that of the NDVI. Therefore, the GOSIF could capture the effects of drought on the grain yield better than the NDVI. As the drought that occurred during 2009–2010 had greater effects over the southern part of China than in other regions in China, the percentage changes in the per-unit grain yield in the NEP, NCP, LP, and QTP subregions did not decrease compared with the corresponding mean annual values. It is worth noting that although the SC region is located in southern China, the percentage change rate in the NDVI and SIF increased. Previous studies showed that the SC region was less affected by drought due to climate background, soil type, and river-network distribution [44,45] during 2009–2010; therefore, the percentage change rate in the NDVI and SIF increased.

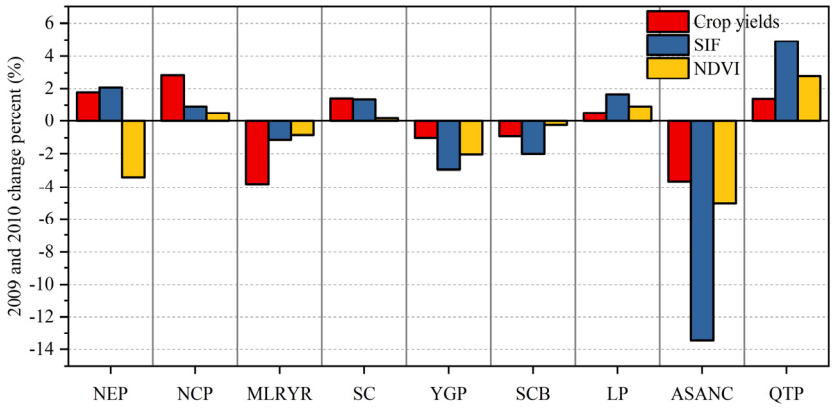

Figure 7. Percentage changes in the per-unit grain yield/SIF/NDVI in the 2009–2010 drought year compared with the corresponding 2001–2019 mean annual values.

4. Discussion

4.1. Differences between SIF and NDVI

By analyzing the consistency between the SIF and NDVI (see Section 3.1), we recorded large differences between these indices in the southeastern and southwestern parts of China (Figure 3). High vegetation-cover levels have been recorded in the southeastern and southwestern parts of China [5,46]. Previous studies have shown that in areas with high vegetation coverage, the NDVI reaches saturation [47,48], which may lead to poor consistency between the NDVI and the SIF. The results obtained in the consistency comparisons between the SIF and the NDVI in different seasons indicated that the relationship between the SIF and the NDVI was less consistent during summer than during autumn or spring (Figures 3 and 4). Cui et al. [49] found that the photosynthetic intensity of vegetation could have a positive linear relationship with the leaf area. As the leaf area increases from spring to summer and decreases from summer to autumn, with a maximum value in summer [13], the differences between the NDVI and the SIF may have been consistent due to the leaf area changes that occur in spring and autumn [32]. However, smaller changes were recorded in the leaf area of vegetation during summer than in other seasons [49]. When the leaf area remains stable, NDVI changes can be small, while the changes in photosynthesis that occur during summer could provide more information on influential factors, such as solar radiation [50] and drought conditions [28]. Therefore, the SIF had a better performance than the NDVI in monitoring the physiological state of the vegetation during summer.

In previous investigations, the NDVI generally underestimated the vegetation dynamics at high vegetation-cover levels [51–54]. Figure 8 shows the relationship obtained between the NDVI and the SIF when applied to forest vegetation areas. In regions where

the vegetation had lower coverage levels (NDVI values not greater than 0.60), good relationships between the SIF and the NDVI were found; by contrast, in regions where the vegetation had higher coverage levels (NDVI values greater than 0.60), poor relationships between the SIF and the NDVI were found (Figure 8a). The distributions of the SIF and the NDVI also revealed differences between the two indices. The SIF distribution fitted a normal distribution better than the NDVI distribution (Figure 8b). In addition, NDVI-based vegetation monitoring corresponds to the reflectance of leaves to radiation, while SIF-based vegetation monitoring is related to photosynthetic intensity. The reflectance changes that occur in evergreen forests are smaller than those of deciduous forests; therefore, the correlations between NDVI and SIF are smaller in evergreen forest areas than in deciduous forest areas.

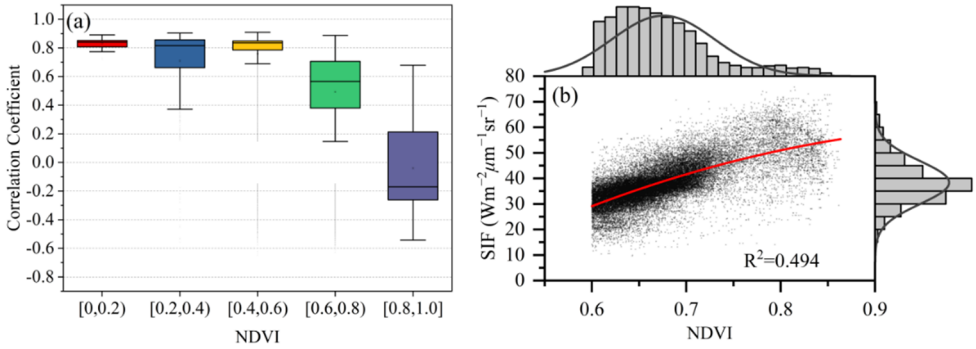

Figure 8. (**a**) The correlation coefficients obtained between the SIF and the NDVI at different NDVI intervals for the whole of China; (**b**) the relationships between the NDVI and the SIF obtained in high-coverage-level forest vegetation areas.

4.2. Reasons for the Different Performances of SIF and NDVI in GPP and Grain-Yield Monitoring

The comparison between the NDVI and SIF results (see Sections 3.2 and 3.3) indicated that the SIF performed better than NDVI when applied to the GPP and grain-yield monitoring (Figures 4 and 5). Previous studies have analyzed various characteristics of vegetation-monitoring indicators. By estimating the performances of indicators when monitoring vegetation characteristics, Chen et al. [32] reported that the SIF had a more significant linear relationship with the GPP than the NDVI did with the NCP. The significant relationship between the SIF and the GPP was also investigated by Ma et al. [55] on a monthly scale in China. The results from these studies were confirmed and expanded upon by our results. Wang et al. [34] pointed out that applying the SIF to urban mixed forest and cropland ecosystems would result in a better ability to indicate the growing season's end date than the application of the NDVI. Chang et al. [56] analyzed the ability of vegetation-monitoring indicators to reveal phenology characterizations in high-latitude and snow-covered forests (including North America and North Eurasia), and the results indicated that GPP and SIF had a high level of consistency in determining the start of the growing season. Chang et al. [21] found that the SIF had a higher level of performance than the NDVI when monitoring crop characteristics during weekly seasonal campaigns. This result agreed with our consistency results obtained from the NDVI, SIF, and per-unit grain yield (Figure 7). Although Jeong et al. [33] found that the SIF and the GPP indicated similar vegetation phenology characterizations in different seasons, the NDVI usually overestimated the GPP compared to the observations, especially during spring and autumn, over high-latitude areas. Jeong et al. [33] also advised that the simulations of the phenological characteristics of vegetation physiology (by SIF) and structure (by NDVI) should be separated to reduce biases in the simulated GPP results. Our results showed that the correlation between the SIF and the GPP was greater than that between the NDVI and the GPP in different seasons; this may have been due to the vegetation producing organic substances via photosynthesis [4,57]. Due to the physiological processes of plants, organic substances can be converted into vegetation biomass (GPP or grain yields). In particular,

the key to cropland vegetation simulations might be considering the amount of organic matter present rather than the level of vegetation cover [58,59]. Therefore, based on the principle of physiological vegetation characteristics, SIF might be more suitable than NDVI for describing GPP [28] and grain yields [8].

4.3. Limitations

The limitations and uncertainties of the results in this study were highly influenced by the quality of the GPP datasets. The MODIS GPP produces were based on the LUE model. The LUE model relied on many types of ground parameter. Many inaccurate parameters were inputted into the LUE model, which may lead to errors in GPP products [40]. The GPP products obtained by the eddy covariance technique (EC, GPP flux tower) were considered as the most accurate GPP data [60]. However, the sampling area of the flux tower was small (<1 km^2) and its distribution was not uniform, making it difficult to conduct a large-scale evaluation. The mismatch between the observation range of the flux-tower site and the monitoring range of the remote-sensing data was another important reason for the limitation of the GPP flux tower [36]. As more high-resolution satellites are launched and flux-tower data become available, more reliable GPP produces will be obtained in the future to eliminate uncertainties. Therefore, we propose to improve the LUE model or control the quality of the input parameters to improve the accuracy of the MODIS GPP produces. The more precise and reliable GPP products can be used in future research for further detailed analyses and to verify our results.

The spatial resolution and time-series length of the SIF limit its application. GOSIF (0.05°) provides better spatial resolution than other SIF products, providing an unprecedented opportunity to explore the estimation of GPP on large scale. In this study, we explored the relationship between the GOSIF and the GPP/per-unit grain yield among different land-cover types and in different seasons. Based on our results, we believe that GOSIFs have great potential in GPP monitoring and per-unit grain-yield monitoring around the world. However, GOSIF also involves uncertainty, including over meteorological reanalysis data, the quality of OCO-2 SIF, the biases in the enhanced vegetation index, and imperfect modeling methods [36,37]. There are currently no satellites dedicated to SIF observations. Therefore, it is necessary to obtain more accurate SIF data sets in the future. In the future, the availability of long-term SIF observations will help us to better understand the differences between the SIF and the vegetation index (such as NDVI) in reflecting GPP/per-unit grain yield, and improve our understanding of the function of ecosystems under climate change.

In addition, our study only used a correlation analysis to study the relationship between the SIF/NDVI and the per-unit grain yield, and described per-unit grain-yield changes in drought years. Although we provided a link between the SIF/NDVI and per-unit grain yield, further analysis needs to be combined with biophysical models to reveal the potential mechanisms of drought affecting grain yields. Moreover, the responses of different crops to drought are not the same due to the differences in photosynthetic capacity, metabolic capacity, and the required growing periods. This study only briefly analyzed the application of NDVI and SIF in yield monitoring. Future studies can use a drought event as an example to analyze the effects of drought on specific crops (such as rice, corn, and wheat).

5. Conclusions

This study compared the relationships between SIF and NDVI among different land-cover types and in different seasons and evaluated their applicability for monitoring GPP and grain yields in China. The results can provide a reference for the selection of NDVI or SIF as vegetation-monitoring indicators in different applications. The main findings of this study can be summarized as follows.

(1) The NDVI and SIF change trends showed that decreasing vegetation trends were mainly concentrated in the northern part of Xinjiang, in part of the QTP, and in a small

part of northeastern China. The NDVI and SIF were more closely related in all the analyzed land-cover type regions than ENF and EBF areas.

(2) The spatial distribution characteristics of the relationships between the SIF (NDVI) and the GPP were similar among different seasons, and the correlations were smaller in southern China and northwestern China than in the other regions of China. In general, the correlations between the SIF (NDVI) and the GPP were smaller in the forest vegetation regions during summer than in other seasons. Moreover, the SIF had a stronger correlation with the GPP than the NDVI did in different seasons.

(3) The PCC and R^2 values obtained between the SIF and the per-unit grain yield were generally higher than those obtained between the NDVI and the per-unit grain yield. The percentage changes in the per-unit grain yield and SIF were similar, indicating that the SIF could capture the effect of the drought on the grain yields better than the NDVI could.

Furthermore, we also need to be fully aware of the following limitations of this study, which are mainly related to three aspects. First, the temporal extent of the SIF data is still relatively short and, thus, cannot describe long-term vegetation changes. As the temporal extent of the available SIF data is extended, SIF will be more widely used. Second, desert vegetation plays an important role in combating desertification, but neither NDVI nor SIF can effectively reflect the changes in the GPP in BSV regions in the northwestern part of China. It is therefore important that future investigations analyze desert vegetation indicators. Third, the suitable vegetation-indicator selection may differ among different applications. As more high-resolution satellites are launched, more precise and reliable datasets can be used in future research to further analyze and verify our results. Nevertheless, notwithstanding the above limitations, the outcomes of this study can provide a reference for selecting suitable vegetation indicators in future vegetation studies.

Author Contributions: Conceptualization: H.S.; data curation: Z.Z.; formal analysis: Z.Z.; funding acquisition: H.S.; methodology: Z.Z. and Y.D.; supervision: H.S., Q.F. and S.L.; validation: Z.Z., Y.D. and Y.W.; writing—original draft: Z.Z.; writing—reviewing and editing: H.S. and S.L. All authors have read and agreed to the published version of the manuscript.

Funding: This study was supported by National Natural Science Foundation of China (51909117), the Natural Science Foundation of Shenzhen (JCYJ20210324105014039), the Guangdong Provincial Key Laboratory of Soil and Ground Water Pollution Control (2017B030301012), and the State Environmental Protection Key Laboratory of Integrated Surface-Water–Groundwater Pollution Control.

Data Availability Statement: The GOSIF data are available at https://globalecology.unh.edu/data/GOSIF.html, accessed on 21 October 2021. The NDVI and GPP data are available at https://modis.gsfc.nasa.gov/data/, accessed on 21 October 2021. The grain yields and cropland area data recorded from 2001 to 2019 are available at the Ministry of Agriculture and Rural Affairs of China (http://zdscxx.moa.gov.cn:8080/nyb/pc/index.jsp, accessed on 21 October 2021) and the China Statistical Yearbook, published by the National Bureau of statistics (http://www.stats.gov.cn/tjsj/ndsj/, accessed on 21 October 2021).

Conflicts of Interest: The authors declare that they have no known competing financial interests or personal relationships that could have appeared to influence the work reported in this paper.

References

1. Chatterjee, A.; Chatterjee, S.; Smith, B.; Cresswell, J.E.; Basu, P. Predicted thresholds for natural vegetation cover to safeguard pollinator services in agricultural landscapes. *Agric. Ecosyst. Environ.* **2020**, *290*, 106785. [CrossRef]
2. Ciais, P.; Reichstein, M.; Viovy, N.; Granier, A.; Ogée, J.; Allard, V.; Aubinet, M.; Buchmann, N.; Bernhofer, C.; Carrara, A.; et al. Europe-wide reduction in primary productivity caused by the heat and drought in 2003. *Nature* **2005**, *437*, 529–533. [CrossRef] [PubMed]
3. Higgins, S.I.; Scheiter, S. Atmospheric CO2 forces abrupt vegetation shifts locally, but not globally. *Nature* **2012**, *488*, 209–212. [CrossRef]
4. Mohammed, G.H.; Colombo, R.; Middleton, E.M.; Rascher, U.; van der Tol, C.; Nedbal, L.; Goulas, Y.; Pérez-Priego, O.; Damm, A.; Meroni, M.; et al. Remote sensing of solar-induced chlorophyll fluorescence (SIF) in vegetation: 50 years of progress. *Remote Sens. Environ.* **2019**, *231*, 111177. [CrossRef] [PubMed]

5. Zhou, Z.Q.; Ding, Y.B.; Shi, H.Y.; Cai, H.J.; Fu, Q.; Liu, S.N.; Li, T.X. Analysis and prediction of vegetation dynamic changes in China: Past, present and future. *Ecol. Indic.* **2020**, *117*, 106642. [CrossRef]
6. He, L.; Chen, J.M.; Liu, J.; Zheng, T.; Wang, R.; Joiner, J.; Chou, S.; Chen, B.; Liu, Y.; Liu, R.G.; et al. Diverse photosynthetic capacity of global ecosystems mapped by satellite chlorophyll fluorescence measurements. *Remote Sens. Environ.* **2019**, *232*, 111344. [CrossRef]
7. Kern, A.; Barcza, Z.; Marjanovic, H.; Arendas, T.; Fodor, N.; Bonts, P.; Bognar, P.; Lichtenberger, J. Statistical modelling of crop yield in Central Europe using climate data and remote sensing vegetation indices. *Agric. For. Meteorol.* **2018**, *260–261*, 300–320. [CrossRef]
8. Peña-Gallardo, M.; Vicente-Serrano, S.M.; Quiring, S.; Svoboda, M.; Hannaford, J.; Tomas-Burguera, M.; Martín-Hernández, N.; Domínguez-Castro, F.; Kenawy, A.E. Response of crop yield to different time-scales of drought in the United States: Spatio-temporal patterns and climatic and environmental drivers. *Agric. For. Meteorol.* **2019**, *264*, 40–55. [CrossRef]
9. Zhou, J.; Zhang, Z.Q.; Sun, G.; Fang, X.R.; Zha, T.G.; Mcnulty, S.; Chen, J.Q.; Jin, Y.; Noormets, A. Response of ecosystem carbon fluxes to drought events in a poplar plantation in Northern China. *For. Ecol. Manag.* **2013**, *300*, 33–42. [CrossRef]
10. Trabucco, A.; Zomer, R.J.; Bossio, D.A.; van Straaten, O.; Verchot, L.V. Climate change mitigation through afforestation/reforestation: A global analysis of hydrologic impacts with four case studies. *Agric. Ecosyst. Environ.* **2008**, *126*, 81–97. [CrossRef]
11. Jiang, C.; Zhang, H.Y.; Zhang, Z.D.; Wang, D.W. Model-based assessment soil loss by wind and water erosion in China's Loess Plateau: Dynamic change, conservation effectiveness, and strategies for sustainable restoration. *Glob. Planet. Change* **2019**, *172*, 396–413. [CrossRef]
12. Liu, Y.F.; Liu, Y.; Shi, Z.H.; López-Vicente, M.; Wu, G.L. Effectiveness of re-vegetated forest and grassland on soil erosion control in the semi-arid Loess Plateau. *Catena* **2020**, *195*, 104787. [CrossRef]
13. Ye, W.T.; van Dijk, A.I.J.M.; Huete, A.; Yebra, M. Global trends in vegetation seasonality in the GIMMS NDVI3g and their robustness. *Int. J. Appl. Earth Obs.* **2021**, *94*, 102238. [CrossRef]
14. Li, X.; Xiao, J.F. A Global, 0.05-Degree Product of Solar-Induced Chlorophyll Fluorescence Derived from OCO-2, MODIS, and Reanalysis Data. *Remote Sens.* **2019**, *11*, 517. [CrossRef]
15. Wei, T.F.; Shangguan, D.H.; Yi, S.H.; Ding, Y.J. Characteristics and controls of vegetation and diversity changes monitored with an unmanned aerial vehicle (UAV) in the foreland of the Urumqi Glacier No. 1, Tianshan, China. *Sci. Total Environ.* **2021**, *771*, 145433. [CrossRef] [PubMed]
16. Wan, J.Z.; Wang, C.J.; Qu, H.; Liu, R.; Zhang, Z.X. Vulnerability of forest vegetation to anthropogenic climate change in China. *Sci. Total Environ.* **2018**, *621*, 1633–1641. [CrossRef]
17. Yang, J.L.; Ding, J.W.; Xiao, X.M.; Dai, J.H.; Wu, C.Y.; Xia, J.Y.; Zhao, G.S.; Zhao, M.M.; Li, Z.L.; Zhang, Y.; et al. Divergent shifts in peak photosynthesis timing of temperate and alpine grasslands in China. *Remote Sens. Environ.* **2019**, *233*, 111395. [CrossRef]
18. Liu, F.; Wang, C.K.; Wang, X.C. Sampling protocols of specific leaf area for improving accuracy of the estimation of forest leaf area index. *Agric. For. Meteorol.* **2021**, *298–299*, 108286. [CrossRef]
19. Xu, J.T.; Cai, H.J.; Saddique, Q.; Wang, X.Y.; Li, L.; Ma, C.J.; Liu, Y.J. Evaluation and optimization of border irrigation in different irrigation seasons based on temporal variation of infiltration and roughness. *Agric. Water Manag.* **2019**, *214*, 64–77. [CrossRef]
20. Pinzon, J.; Tucker, C. A Non-Stationary 1981–2012 AVHRR NDVI3g Time Series. *Remote Sens.* **2014**, *6*, 6929–6960. [CrossRef]
21. Chang, C.Y.; Zhou, R.Q.; Kria, O.; Marri, S.; Skovira, J.; Gu, L.H.; Sun, Y. An Unmanned Aerial System (UAS) for concurrent measurements of solar-induced chlorophyll fluorescence and hyperspectral reflectance toward improving crop monitoring. *Agric. For. Meteorol.* **2020**, *294*, 108145. [CrossRef]
22. Fan, X.; Liu, Y. A global study of NDVI difference among moderate-resolution satellite sensors. *ISPRS J. Photogramm.* **2016**, *121*, 177–191. [CrossRef]
23. Pengra, B.; Long, J.; Dahal, D.; Stehman, S.V.; Loveland, T.R. A global reference database from very high resolution commercial satellite data and methodology for application to Landsat derived 30 m continuous field tree cover data. *Remote Sens. Environ.* **2015**, *165*, 234–248. [CrossRef]
24. Shi, H.Y.; Chen, J. Characteristics of climate change and its relationship with land use/cover change in Yunnan Province, China. *Int. J. Climatol.* **2018**, *38*, 2520–2537. [CrossRef]
25. Quiring, S.M.; Ganesh, S. Evaluating the utility of the Vegetation Condition Index (VCI) for monitoring meteorological drought in Texas. *Agric. For. Meteorol.* **2010**, *150*, 330–339. [CrossRef]
26. Bento, V.A.; Gouveia, C.M.; DaCamara, C.C.; Trigo, I.F. A climatological assessment of drought impact on vegetation health index. *Agric. For. Meteorol.* **2018**, *259*, 286–295. [CrossRef]
27. Shammi, S.A.; Meng, Q.M. Use time series NDVI and EVI to develop dynamic crop growth metrics for yield modeling. *Ecol. Indic.* **2021**, *121*, 107124. [CrossRef]
28. Chen, S.; Huang, Y.; Wang, G. Detecting drought-induced GPP spatiotemporal variabilities with sun-induced chlorophyll fluorescence during the 2009/2010 droughts in China. *Ecol. Indic.* **2021**, *121*, 107092. [CrossRef]
29. Ding, Y.B.; Xu, J.T.; Wang, X.W.; Peng, X.B.; Cai, H.J. Spatial and temporal effects of drought on Chinese vegetation under different coverage levels. *Sci. Total Environ.* **2020**, *716*, 137166. [CrossRef]
30. Xu, H.J.; Wang, X.P.; Zhao, C.Y.; Yang, X.M. Diverse responses of vegetation growth to meteorological drought across climate zones and land biomes in northern China from 1981 to 2014. *Agric. For. Meteorol.* **2018**, *262*, 1–13. [CrossRef]

31. Liu, Y.; Dang, C.Y.; Yue, H.; Lyu, C.G.; Dang, X.H. Enhanced drought detection and monitoring using sun-induced chlorophyll fluorescence over Hulun Buir Grassland, China. *Sci. Total Environ.* **2021**, *770*, 145271. [CrossRef] [PubMed]
32. Chen, X.J.; Mo, X.G.; Zhang, Y.C.; Sun, Z.G.; Liu, Y.; Hu, S.; Liu, S.X. Drought detection and assessment with solar-induced chlorophyll fluorescence in summer maize growth period over North China Plain. *Ecol. Indic.* **2019**, *104*, 347–356. [CrossRef]
33. Jeong, S.J.; Schimel, D.; Frankenberg, C.; Drewry, D.T.; Fisher, J.B.; Verma, M.; Berry, J.A.; Lee, J.E.; Joiner, J. Application of satellite solar-induced chlorophyll fluorescence to understanding large-scale variations in vegetation phenology and function over northern high latitude forests. *Remote Sens. Environ.* **2017**, *190*, 178–187. [CrossRef]
34. Wang, F.; Chen, B.Z.; Lin, X.F.; Zhang, H.F. Solar-induced chlorophyll fluorescence as an indicator for determining the end date of the vegetation growing season. *Ecol. Indic.* **2020**, *109*, 105755. [CrossRef]
35. Ding, Y.B.; Xu, J.T.; Wang, X.W.; Cai, H.J.; Zhou, Z.Q.; Sun, Y.N.; Shi, H.Y. Propagation of meteorological to hydrological drought for different climate regions in China. *J. Environ. Manag.* **2021**, *283*, 111980. [CrossRef]
36. Qiu, R.N.; Han, G.; Ma, X.; Xu, H.; Shi, T.Q.; Zhang, M. A comparison of OCO-2 SIF, MODIS GPP, and GOSIF data from Gross Primary Production (GPP) estimation and seasonal cycles in North America. *Remote Sens.* **2020**, *12*, 258. [CrossRef]
37. Li, X.; Xiao, J.F. Global climatic controls on interannual variability of ecosystem productivity: Similarities and differences inferred from solar-induced chlorophyll fluorescence and enhanced vegetation index. *Agric. For. Meteorol.* **2020**, *288–289*, 108018. [CrossRef]
38. Shim, C.; Hong, J.; Hong, J.Y.; Kim, Y.; Kang, M.; Thakuri, B.M.; Kim, Y.; Chun, J. Evaluation of MODIS GPP over a complex ecosystem in East Asia: A case study at Gwangneung flux tower in Korea. *Adv. Space Res.* **2014**, *54*, 2296–2308. [CrossRef]
39. Heinsch, F.A.; Reeves, M.; Votava, P.; Kang, S.; Milesi, C.; Zhao, M.; Glassy, J.; Jolly, W.M.; Kimball, J.S.; Nemannpi, R.R.; et al. *User's Guide GPP and NPP (MOD17A2/A3) Products, NASA MODIS Land Algorithm*; MOD17 User's Guide; University of Montana: Missoula, MT, USA, 2003; pp. 1–57.
40. Zhao, M.S.; Heinsch, F.A.; Nemani, R.R.; Running, S.W. Improvements of the MODIS terrestrial gross and net primary production global data set. *Remote Sens. Environ.* **2005**, *95*, 164–176. [CrossRef]
41. Wang, S.H.; Zhang, L.F.; Huang, C.P.; Qiao, N. An NDVI-Based Vegetation Phenology Is Improved to be More Consistent with Photosynthesis Dynamics through Applying a Light Use Efficiency Model over Boreal High-Latitude Forests. *Remote Sens.* **2017**, *9*, 695. [CrossRef]
42. Tian, F.; Wu, J.J.; Liu, L.Z.; Leng, S.; Yang, J.H.; Zhao, W.H.; Shen, Q. Exceptional drought across Southeastern Australia caused by extreme lack of precipitation and its impacts on NDVI and SIF in 2018. *Remote Sens.* **2019**, *12*, 54. [CrossRef]
43. Zhou, Z.Q.; Shi, H.Y.; Fu, Q.; Ding, Y.B.; Li, T.X.; Wang, Y.; Liu, S.N. Characteristics of propagation from meteorological drought to hydrological drought in the Pearl River Basin. *J. Geophys. Res. Atmos.* **2021**, *126*, e2020JD033959. [CrossRef]
44. Wang, S.P.; Wang, J.S.; Feng, J.Y. Drought in China and its impact and causes in the autumn of 2010. *J. Arid. Meteorol.* **2010**, *4*, 499–504. (In Chinese)
45. Wang, J.S.; Zhang, Q.; Wang, S.P.; Wang, Y.; Wang, J.; Yao, Y.B.; Ren, Y.L. Characteristic analysis of drought disaster chain in Southwest and South China. *J. Arid. Meteorol.* **2015**, *33*, 187–194.
46. Xu, C.; McDowell, N.G.; Fisher, R.A.; Wei, L.; Sevanto, S.; Chrisrtoffersen, B.O.; Wang, E.S.; Middleton, R.S. Increasing impacts of extreme droughts on vegetation productivity under climate change. *Nat. Clim. Chang.* **2019**, *9*, 948–953. [CrossRef]
47. Wang, G.Q.; Liu, S.M.; Liu, T.X.; Fu, Z.Y.; Yu, J.S.; Xue, B.L. Modelling above-ground biomass based on vegetation indexes: A modified approach for biomass estimation in semi-arid grasslands. *Int. J. Remote Sens.* **2019**, *40*, 3835–3854. [CrossRef]
48. Liu, F.; Qin, Q.M.; Zhan, Z.M. A novel dynamic stretching solution to eliminate saturation effect in NDVI and its application in drought monitoring. *Chin. Geogr. Sci.* **2012**, *22*, 683–694. [CrossRef]
49. Cui, T.X.; Sun, R.; Xiao, Z.Q.; Liang, Z.Y.; Wang, J. Simulating spatially distributed solar-induced chlorophyll fluorescence using a BEPS-SCOPE coupling framework. *Agric. For. Meteorol.* **2020**, *295*, 108169. [CrossRef]
50. Wu, W.; Tang, X.P.; Yang, C.; Guo, N.J.; Liu, H.B. Spatial estimation of monthly mean daily sunshine hours and solar radiation across mainland China. *Renew. Energy* **2013**, *57*, 546–553. [CrossRef]
51. Carlson, T.N.; Ripley, D.A. On the relation between NDVI, fractional vegetation cover, and leaf area index. *Remote Sens. Environ.* **1997**, *62*, 241–252. [CrossRef]
52. Fensholt, R.; Proud, S.R. Evaluation of Earth Observation based global long term vegetation trends—Comparing GIMMS and MODIS global NDVI time series. *Remote Sens. Environ.* **2012**, *119*, 131–147. [CrossRef]
53. Hasegawa, K.; Matsuyama, H.; Tsuzuki, H.; Sweda, T. Improving the estimation of leaf area index by using remotely sensed NDVI with BRDF signatures. *Remote Sens. Environ.* **2010**, *114*, 514–519. [CrossRef]
54. Rokni, K.; Musa, T.A. Normalized difference vegetation change index: A technique for detecting vegetation changes using Landsat imagery. *Catena* **2019**, *178*, 59–63. [CrossRef]
55. Ma, J.; Xiao, X.; Zhang, Y.; Chen, B.; Zhao, B. Spatial-temporal consistency between gross primary productivity and solar-induced chlorophyll fluorescence of vegetation in China during 2007–2014. *Sci. Total Environ.* **2018**, *639*, 1241–1253. [CrossRef]
56. Chang, Q.; Xiao, X.M.; Jiao, W.Z.; Wu, X.C.; Doughty, R.; Wang, J.; Du, L.; Zou, Z.H.; Qin, Y.W. Assessing consistency of spring phenology of snow-covered forests as estimated by vegetation indices, gross primary production, and solar-induced chlorophyll fluorescence. *Agric. For. Meteorol.* **2019**, *275*, 305–316. [CrossRef]
57. Guo, P.P.; Guo, K.J.; Ren, Y.; Shi, Y.; Chang, J.; Tani, A.; Ge, Y. Biogenic volatile organic compound emissions in relation to plant carbon fixation in a subtropical urban–rural complex. *Landsc. Urban Plan.* **2013**, *119*, 74–84. [CrossRef]

58. Xu, J.T.; Cai, H.J.; Wang, X.Y.; Ma, C.G.; Lu, Y.J.; Ding, Y.B.; Wang, X.W.; Chen, H.; Wang, Y.F.; Saddique, Q. Exploring optimal irrigation and nitrogen fertilization in a winter wheat-summer maize rotation system for improving crop yield and reducing water and nitrogen leaching. *Agric. Water Manag.* **2020**, *228*, 105904. [CrossRef]
59. Zhou, Z.Q.; Shi, H.Y.; Fu, Q.; Li, T.X.; Gan, T.Y.; Liu, S.N. Assessing spatiotemporal characteristics of drought and its effects on climate-induced yield of maize in Northeast China. *J. Hydrol.* **2020**, *588*, 125097. [CrossRef]
60. Yang, X.; Tang, J.; Mustard, J.F.; Lee, J.E.; Rossini, M.; Joiner, J.; Munger, J.W.; Kornfeld, A.; Richardson, A.D. Solar-induced chlorophyll fluorescence that correlates with canopy photosynthesis on diurnal and seasonal scales in a temperate deciduous forest. *Geophys. Res. Lett.* **2015**, *42*, 2977–2987. [CrossRef]